Wavefront Controls for a Large Submillimeter-Wave Observatory

David Redding[1*a], John Z. Lou[a], Andy Kissil[a], Matt Bradford[a], Steve Padin[b] and David Woody[b]
[a]Jet Propulsion Laboratory, California Institute of Technology, Pasadena CA 91109;
[b]California Institute of Technology, Pasadena CA 91106

ABSTRACT

The 25-m aperture Cornell Caltech Atacama Telescope (CCAT) will have a primary mirror that is divided into 162 individual segments, each of which is equipped with 3 positioning actuators. This paper presents a mathematical description of the telescope, its actuators and sensors, and uses it to derive control laws for figure maintenance. A Kalman Filter-based Optical State Estimator is used to continuously estimate the aberrations of the telescope; these are used in a state-feedback controller to maintain image quality. This approach provides the means to correct for the optical effects of errors that occur in un-actuated degrees of freedom, such as lateral translations of the segments. The control laws are exercised in Monte Carlo and covariance analysis, to bound the closed-loop performance of the telescope and to conduct control design trades.

Keywords: Segmented mirror, wavefront control, edge sensors, Kalman filter.

1. INTRODUCTION

The 25-m aperture Cornell Caltech Atacama Telescope (CCAT) will be sited at an altitude of 5600 m in the Atacama Desert. It will have a primary mirror assembled from 162 "keystone" segments, each of which is equipped with 3 rigid-body actuators. These will be used to move the segments, so as to counter deformations from temperature changes and the varying gravity effects that come with pointing changes. The baseline control approach is to determine the best positioning of the segments using submillimeter-wave shearing interferometry, and then to maintain optical performance during operations using feed-forward, look-up table controls. This approach may not be adequate for operation at the shorter submillimeter wavelengths, however.

This paper presents an alternative: a Wavefront Compensation controller that uses innovative optical sensors to measure segment-to-segment displacements and determine actuator commands that maintain good optical quality. The controller uses a Kalman filter to estimate the full optical state of the telescope, including 6 degrees of freedom (DOF) of change for each segment, and to predict the Wavefront Error (WFE) that results from these changes. Actuator controls are computed to minimize this WFE at each time step, using only the 3 DOF provided by the actuators. This approach is able to partly compensate the WFE due to motions in the uncontrolled DOFs, resulting in better performance than approaches that simply seek to null the sensor signals.

The estimator and controller are based on a detailed mathematical model of the telescope, currently based on structural and optical computer models, but which will ultimately be determined by direct calibration. These models are summarized in Section 3, following a summary of nomenclature in Section 2. The estimator and controller are derived in Sections 4-6, and example results are presented in Section 7.

2. NOMENCLATURE

x_R, rigid-body state of each optic or optical assembly, $[x_R]$ = (6*nopt,1)
x_D, segment deformation state, $[x_D]$ = (ndef*nseg, 1)
u_R, segment rigid body control command, $[u_R]$ = (6*nseg, 1)
u_{SM}, SM rigid body control command, $[u_{SM}]$ = (5, 1)

* david.c.redding@jpl.nasa.gov

u_c, pointing control command, $[u_c] = (2, 1)$
δT, temperature change, $[\delta T]$ = (nT*nseg, 1)
x, process noise, $[dT] = (x, 1)$
l, optical edge sensor measurements, $[l]$ = (2*nl,1)
δl, optical edge measurement noise, $[\delta l]$ = (2*nl,1)
w, wavefront, $[w]$ = (nray,1)
w_{Atm}, wavefront error due to atmosphere
δw, wavefront measurement noise, $[\delta w]$ = (nray,1)
OPD, Optical Path Difference matrix
c, ray centroid, $[c] = (2,1)$
δc, pointing measurement noise, $[\delta c] = (2,1)$
K, estimator gain
c_{wu}, control weighting coefficient
i, time index
Capitalized variable signifies the covariance of that variable
Bar over a variable signifies a predicted value (prior to incorporation of current measurement data)
Hat over a variable signifies current estimate
Squiggle over a variable signifies current estimate error

Figure 1. CCAT overview.

3. CCAT MODEL

A detailed integrated optics/structures/thermal computer model of CCAT is being built, to aid in design studies of the CCAT telescope.[1] The optics part of the CCAT integrated model has been built using the JPL MACOS code.[4] This model includes each optic, i.e., 162 primary mirror (PM) segments, the secondary mirror (SM), back-end optics and detector, as a separate body capable of displacement in 3 rotational and 3 translational DOFs. Perturbations from their ideal designed positions and orientations are captured in the "rigid-body optical state," x_{Ri}, a vector of dimension 948x1, evaluated at the ith time interval. The state is defined in coordinates local to each optic, centered at the pole of the optic, and oriented along the local radial, tangential and normal directions.

The optics have thermal deformations and fabrication errors, which effects are included in the "deformation optical state," x_{Di}. Thermal modes are computed using the structures part of the CCAT integrated model, using NASTRAN. The thermal modes are used to compute optical surface deformations at node points on a grid defined in local coordinates for each optic. The total optical state vector combines these elements into a single vector.

The full state at the *i*th time interval combines the rigid and deformation states of all of the optics into a single vector:

$$x_i = \begin{bmatrix} x_{Ri} \\ x_{Di} \end{bmatrix} \tag{1}$$

Each segment is equipped with 3 actuators, which control its tip, tilt and piston in the same local coordinate frames. Actuator-driven segment perturbations are denoted u_R. The SM is equipped with 6 actuators; its perturbations are u_{SM}.

The full dynamics of the CCAT structure do not need to be included in the control derivation model, though ultimately they are included in the more detailed system performance simulation: the "truth model." For control design purposes it is sufficient to envelope the behavior of the CCAT structure, using a process noise term ξ to introduce random state changes; and using coupled disturbance modes *T*, including thermal modes of the segments, thermal modes of the telescope structures, the effects of gravity as the telescope pointing changes, and other global effects. This results in a state transition equation that does not include any dynamics:

$$x_i = x_{i-1} + \frac{\partial x}{\partial u_R} u_{Ri} + \frac{\partial x}{\partial u_{SM}} u_{SMi} + \frac{\partial x}{\partial T} T_i + \xi_i \tag{2}$$

That is, the state at the i+1th time interval is equal to the state at the ith time interval, plus changes induced by actuator motions, changes due to disturbance modes, and changes due to the process noise ξ. The coupling of the actuations to the state are through the $\partial x / \partial u$, which are simple mapping matrices. The mode sensitivities $\partial x / \partial T$ are generated using the CCAT FEA model. Temperature modes used include segment temperature soaks, substructure gradients and substructure soaks. Gravity sag modes are computed for different elevation angles. The T are used to provide initial conditions for the state; they are also varied with time to provide representative coupled disturbances for the CCAT controller to correct.

Changes in the state *x* have optical effects: wavefront *w* degrades; the telescope pointing *c* wanders. The CCAT MACOS model computes these optical effects by perturbing the position and shape of each optic, and then tracing rays through the optical system, from a star at infinity, past each optic to the detector. The wavefront *w* is the vectorized form of the Optical Path Difference (OPD) matrix: a map of the wavefront (WF) across the pupil, evaluated at an exit pupil conjugate to the PM, which defines the entrance pupil – see Figure 2. The pointing error centroid *c* is computed as the centroid of all of the rays at the detector. The MACOS model includes atmospheric seeing effects w_{Atm} and c_{Atm} as well.

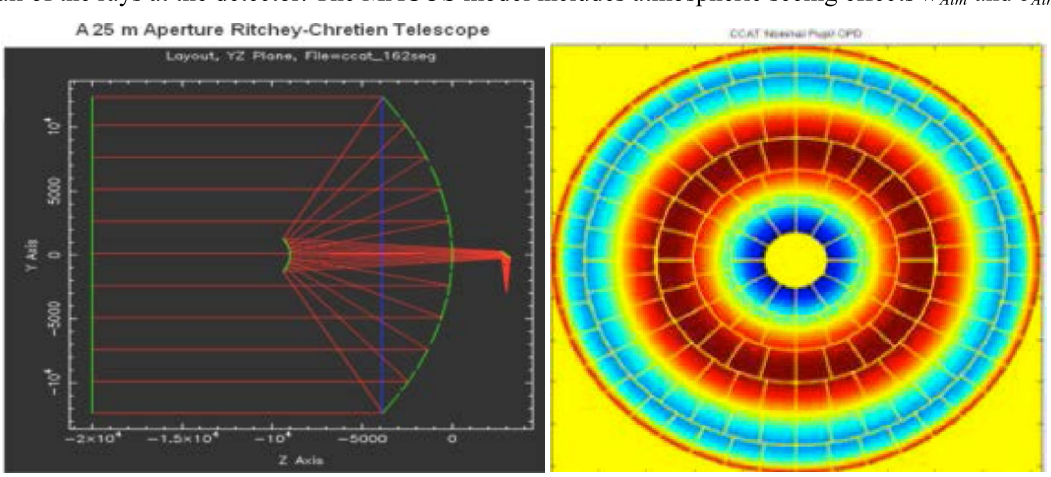

Figure 2. CCAT ray-trace (left) and nominal OPD showing PM segmentation.

For the small motions typical of a controlled telescope, the MACOS model can be linearized, and the effect of the state on the optics can be expressed in matrix form, as:

$$w_i = \frac{\partial w}{\partial x} x_i + w_{Atm} + w_0 \tag{3}$$

$$c_i = \frac{\partial c}{\partial x} x_i + c_{Atm} + c_0 \tag{4}$$

That is, the WF w is equal to the nominal WF w_0 plus the optical effects of the perturbations x, plus the effects of atmospheric turbulence w_{Atm} (small in the submillimeter); similarly for the pointing c. Here MACOS is used to generate the optical sensitivities $\partial w / \partial x$ and $\partial c / \partial x$, following the theory of [5]. This provides linear optical models that predict the WFE and pointing error using matrix operations rather than a full ray-trace; such models are highly accurate for the small state excursions typical of a controlled telescope. The optical sensitivities are also important in the derivations of the controller – see below.

The RMS Wavefront Error (WFE) is computed as the RMS of w_i.

Changes in the state x also impact the outputs of the *measurements* that are used for control. In this paper we consider 3 types of measurement. The first is a direct measurement of the WFE, which can be obtained by WF sensing, or using the shearing interferometry technique discussed in [7]. The WF measurement equation takes the form (assuming fully unwrapped phase):

$$w_{mi} = w_i + \delta w_i = \frac{\partial w}{\partial x} x_i + w_{Atm} + w_0 + \delta w \tag{5}$$

The second type of measurement is made using optical edge sensors. The CCAT edge sensors have 2 parts: a collimated light source located on one segment; and a CCD camera located on the adjacent segment – see Figure 3. Translational or rotational motions of one segment relative to the other cause lateral displacement of the light beam, which is measured by the CCD in 2 axes: in the "z" or local surface normal direction; and "y," parallel to the mirror surface, as described in [6]. Optical edge sensors are placed as shown in Figure 3, with approximately 2 sensors per segment-to-segment edge, and a total of 624 sensors, each sensing in 2 axes for a total of 1248 measurements. Design parameters governing edge sensor performance include the mounting position below the surface and the radial position of each sensor.

The edge sensor measurement equation takes the form:

$$l_i = \frac{\partial l}{\partial x} x_i + l_0 + \delta l_i \tag{6}$$

Here the $\partial l / \partial x$ sensitivities capture the kinematics of the sensors. The l_0 vector represents the static offset of the edge sensors, which can be calibrated. Optical edge sensor measurements will be made at a frequency of 0.1 to 1 Hz.

The third type of measurement is the telescope pointing measurement, made using an off-axis guide star and a separate pointing camera. For this analysis, we assume that the pointing camera provides a measurement to be directly compared to an image at the center of the CCAT field. Unlike the optical edge sensor measurement, which is local to the PM and insensitive to global motions of the optics, c captures effects of all the optics as they affect pointing. The pointing measurement equation is:

$$c_i = \frac{\partial c}{\partial x} x_i + c_{Atm} + c_0 + \delta c_i \tag{7}$$

Pointing measurements will be conducted at a lower rate than optical edge sensor measurements, at 0.001 to 0.01 Hz.

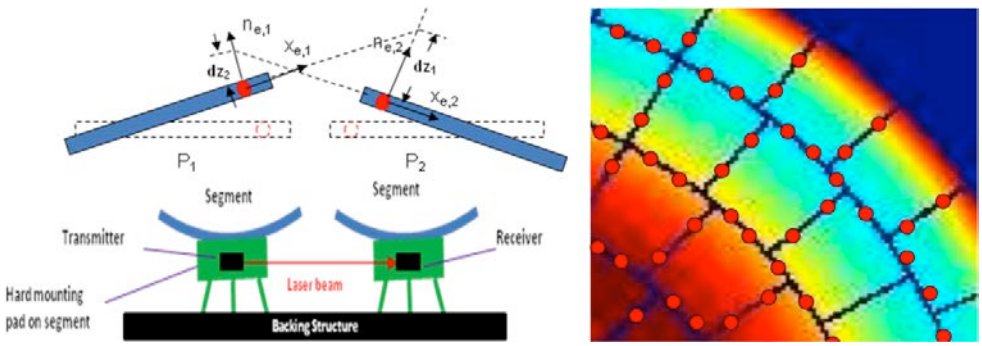

Figure 3. Optical edge sensor sensor geometry.

4. SIMULATION AND COVARIANCE ANALYSIS

The performance of the 25-m CCAT can be bounded from the model equations outlined above, using simulation techniques and covariance analysis. Covariance analysis forms the basis of the CCAT Optical State Estimator discussed in the next Section.

In simulation, telescope performance is computed for a for a particular case, by initializing the state $x = x_0$ with random values consistent with the expected alignment and figure quality of the telescope, and then integrating the state forward in time using the transition equation (Eq. 2). At each time step, new state noise values ξ are added, and values for w, l and c are computed. New controls (with sensing and actuation errors) can be fed back into the state via actuations u. The simulation is run until a steady-state performance is reached. The error in the final performance is a function of the particular errors and noise values that drive it.

Monte Carlo analysis runs many simulations, each with the noise and errors generated using the same statistics, but with different particular realizations of these statistics, and then takes statistics on the results of all of the simulations, to understand the likely performance of a telescope with those particular component error statistics. By changing the component statistics, running more simulations and assessing those results, general conclusions can be drawn on performance as a function of the component error and noise performance statistics. Monte Carlo simulation and related simulation-based techniques are powerful tools, especially where statistics are not gaussian or the plant is nonlinear.

In covariance analysis, rather than conducting many simulations and then taking statistics on the results, the error statistics (in the form of covariance matrices) are propagated directly. Covariance analysis of a linear system provides the same result as Monte Carlo analysis, but with a single evaluation. Covariance analysis assumes that the errors in x and u, the process noise ξ, and the measurement errors ν, are gaussian random variables, which is a good assumption for the small errors typical of telescopes. The errors are treated as zero-mean, by incorporating systematic effects into the underlying models. The process defined by these assumptions is a Markov process [8].

For a linear gaussian random vector x, the following general transformation holds [8]. If a vector $y = H\,x$, then y is also a linear gaussian random vector, with covariance Y, where

$$Y = HXH^T \tag{8}$$

In general we will denote the covariance of a random vector as the capital letter of that variable. Thus cov(x) = X, cov(w) = W, cov(ν) = N. Also, cov(δu) = U, cov(ξ) = Ξ, etc. Applying the rule of Eq. 8 to Eq. 5, we get the state covariance transition equation:

$$X_{i+1} = X_i + \frac{\partial x}{\partial u_R} U_{Ri} \left[\frac{\partial x}{\partial u_R} \right]^T + \frac{\partial x}{\partial u_{SM}} U_{SMi} \left[\frac{\partial x}{\partial u_{SM}} \right]_i^T + \Xi_i \tag{9}$$

This is a discrete Lyapunov equation [8]. The covariance of the ith wavefront is:

$$W_i = \frac{\partial w}{\partial x} x_i \left[\frac{\partial w}{\partial x} \right]^T + W_{Atm} \tag{10}$$

The corresponding RMS WF error is

$$WFE_i = \sqrt{trace((W_i) / n_{ray})} \tag{11}$$

Here n_{ray} is the number of WF samples. Similar algebra is applied to develop expressions for the full closed-loop control WFE in the next Section.

Initial state errors x_0 will typically be generated from a systematic error (δT, say) which produces a systematic, correlated but deterministic global shape change, and a random term that captures uncorrelated effects such as mounting errors. The *initial* covariance X_0 is therefore uncorrelated, diagonal, with the diagonal elements equal to the variance of the corresponding state as determined from component-level specifications. If σ_i is the standard deviation or "1-sigma" error expected for the initial x_i state vector element, then the corresponding entry in X_0 is:

$$X_0(i,i) = 1 / \sigma_i^2 \tag{12}$$

The state covariance matrix X_{i+1} is diagonal only at the initial condition: a single iteration of the control derived below cause the states to become correlated. The optical edge sensor measurement errors have a calibrateable static offset l_0 and uncorrelated measurement noise δl, with standard deviation σ_L, so that the covariance L is:

$$L_0 = (1 / \sigma_L^2) I \tag{13}$$

Here σ_L is the (scalar) standard deviation of the error expected for optical edge sensor measurements, and I is the identity matrix of dimension n_{ray} by n_{ray}. Similar expressions govern the other measurement covariances.

5. OPTICAL STATE ESTIMATOR

The optical edge sensor measurements l (and c and w when available), can be used to estimate the optical state x of the telescope at any particular time; and that estimate can be used to compute new controls u_R and u_{SM}. This is the function of the Optical State Estimator (OSE): to take in all of the available data, and to process it to determine the underlying optical state x of the telescope. The data that is continuously available includes the measurements l and their covariance L; pointing measurements c with covariance C; actuations u_R and u_{SM} and their error covariances U_R and U_{SM}; and the covariance of the process noise, Ξ.

The OSE combines this data with a prediction of the state based on the previous state estimate to carry over information from earlier measurements. The formally optimal way to do this is by Kalman Filter techniques: weighted least-squares, where the estimate weights the measurements and the prior knowledge using the covariance matrices associated with each term to find the most likely state estimate. [8]

The Kalman Filter (KF) is a Maximum-Likelihood linear system estimator in recursive form, which allows it to produce estimates that are optimal at the time each new measurement is taken, while preserving the value of all previous measurements. The KF is a predictor-corrector estimator, where at each measurement we make a *prediction* of the measurement, based on the information we had at the last measurement, and compare that to the actual current measurement. The difference of the predicted and actual measurements, termed the *innovation*, is multiplied by a gain matrix and fed back to update the estimate. The gains are weighted by the covariances of the measurement and prior-estimate errors, so as to achieve an optimal blending of prior and current information.

The prediction is made by taking the estimate computed at the preceding time step and simply projecting it forward in time using Eq. 2. We know the value of the control we commanded, so that goes into the prediction as well. The predicted measurement is then calculated by projecting the predicted state to the WF space using Eq. 3. Denoting the predicted state at time i with an over-bar as , and the estimated state with a hat, as , the predicted state is:

$$\bar{x}_{Ri+1} = \hat{x}_{Ri} + \frac{\partial x_R}{\partial u_R} u_{Ri} \tag{14}$$

The predicted measurement is thus:

$$\bar{l}_i = \frac{\partial l}{\partial x}\bar{x}_i \tag{15}$$

The new state estimate is simply the prediction plus the innovation weighted by a gain matrix K_i:

$$\hat{x}_{Ri} = \bar{x}_{Ri} + K_{li}\left(l_i - \bar{l}_i\right) \tag{16}$$

The gain balances the contribution of the innovation to the current estimate as the ratio of the error in the predicted state, as captured in the predicted-state covariance P_i, to the error in the measurement projected back to the state space via the transpose of the measurement matrix. We treat the actuator commands as known signals with a measurement error equal to the actuation noise projected to the WF space. The error in the measurement is the covariance matrix R_i, which includes the WF measurement error and the actuation error . The gain is:

$$K_{li} = P_{li}\left(\frac{\partial l}{\partial x_R}\right)^T R_{li}^{-1} \tag{17}$$

Note that the gain matrix K_{li} changes with every time step, which can impose a large computational burden on the OSE. In practice, however, K will quickly approach a nearly static steady state, so that it is possible to precompute a set of K_i matrices for the various different control conditions, and use them while those conditions obtain. The factors that cause K_i to vary include variations in the noise covariances L and C.

The measurement error covariance, which captures the uncertainty in both the actuation and the measurement, is:

$$R_{li} = \frac{\partial l}{\partial x_R}\frac{\partial x_R}{\partial u_R}U_i\left(\frac{\partial l}{\partial x_R}\frac{\partial x_R}{\partial u_R}\right)^T + L_i \tag{18}$$

The error in the estimate is captured by its covariance Pi, which combines the measurement and predicted-state error covariances Ri and Mi in the state space, as:

$$P_{li} = \left[\left(\frac{\partial l}{\partial x_R}\right)^T R_{li}\frac{\partial l}{\partial x_R} + M_i^{-1}\right]^{-1} = \mathrm{cov}(\hat{x}_{Ri}) \tag{19}$$

The covariance of the predicted state is computed based on the covariances of the error in the previous estimate, projected forward to the current time:

$$M_{i+1} = P_i + \frac{\partial x}{\partial u_R}U_i\left(\frac{\partial x}{\partial u_R}\right)^T + \Xi_i \tag{20}$$

For gaussian normal random processes, the KF estimator of Eq. 16 produces optimal estimates, in the sense that they make the best possible use of the available information, producing estimates with minimal error. In fact, the KF defines the Cramer-Rao bound for such processes [8]. In practical problems the KF assumptions are not always precisely met. The statistics of the processes may not be normal or stationary, the plant may not be truly linear. Many extensions to the KF have been developed to deal with specific situations of this type. However, for small deviations from the assumptions underlying the KF, the KF provides an excellent, though not precisely optimal, tool.

Equations 14-20 define the KF updates provided by the LADD sensors, which occur at every cycle of the OSE. Other measurements, namely the pointing measurements c and the WF measurements w are incorporated in the same way, but at different times: the pointing measurements will be made every 10-1,000 cycles of the OSE; the WF measurements perhaps once a week. When such measurements are available, they are used to update the state x in exactly the same way. For example, when a pointing measurement is available, the updated state estimate is:

$$\hat{x}_{Ri} = \bar{x}_{Ri} + K_{ci}\left(c_i - \bar{c}_i\right) \tag{21}$$

The gain and updated state estimate error covariance are:

$$K_{ci} = P_{ci}\left(\frac{\partial c}{\partial x_R}\right)^T C_{ci}^{-1} \tag{22}$$

$$P_{ci} = \left[\left(\frac{\partial c}{\partial x_R}\right)^T R_{ci}\frac{\partial c}{\partial x_R}\right]^{-1} = \mathrm{cov}(\hat{x}_{Ri}) \tag{23}$$

Similar results obtain for WF updates through measurements of w.

To illustrate the effect of the gain matrix K in balancing prior estimates versus current measurements, it is useful to consider 2 extreme cases. The first case occurs when the error in the prior estimate is very small, and very much smaller than the measurement noise, so that $P_i \ast 0$. Then $K_i \ast 0$, and the estimate is simply the prediction:

$$\hat{x}_i \rightarrow \bar{x}_i \tag{21}$$

The other extreme case occurs when the combined measurement noise is very much less than the error in the prior estimate. The gain (Eq. 14) can be rewritten using the inversion lemma as:

$$K_{li} = P_{li}\left(\frac{\partial l}{\partial x_R}\right)^T\left[R_{li} + \frac{\partial l}{\partial x}P_i\left(\frac{\partial l}{\partial x}\right)^T\right]^{-1} \tag{22}$$

Now when $R_i \ast 0$,

$$K_i \rightarrow \left[\left(\frac{\partial l}{\partial x}\right)^T\frac{\partial l}{\partial x}\right]^{-1}\left(\frac{\partial l}{\partial x}\right)^T \tag{23}$$

which is the familiar pseudo-inverse solution of the measurement equation.

The best performance for any real case, where prior knowledge error and measurement noise are in more nearly the same, is obtained when the covariances X_0, Ξ, L, and C are accurately specified, as they determine the balance between measurement and prior knowledge for the OSE. If the measurement noise covariance reflects an assumed small measurement error, but the actual measurement error is large, for instance, The K_i matrix will couple too much of the measurement error into the state estimate, and performance of the OSE will be degraded.

6. WAVEFRONT CONTROLLER

The best way to control the WFE is to directly measure w and use those measurements to compute new control values. The cost function for this form of control is:

$$\min_{u_R} J = w^T w + c_{wu} u_R{}^T u_R \tag{24}$$

There are 2 terms here, balanced by a scalar coefficient c_{wu}. The first term is the square of the WF; the second is the square of the control effort between the ith and the i-1th iteration. The coefficient can be tuned to balance the control effort against the WFE, a useful knob to turn in modulating the control response. The control law that satisfies this cost function is:

$$u_{Ri} = -\left[c_{wu} I + \left(\frac{\partial w}{\partial x_R} \frac{\partial x_R}{\partial u_R} \right)^T \frac{\partial w}{\partial x_R} \frac{\partial x_R}{\partial u_R} \right]^{-1} \left(\frac{\partial w}{\partial x_R} \frac{\partial x_R}{\partial u_R} \right)^T w_i \tag{25}$$

Continuous direct measurement of w is not provided under the current CCAT baseline. Instead, the state estimate produced by the OSE can be used to estimate w:

$$\hat{w}_i = \frac{\partial w}{\partial x} \hat{x}_i \tag{26}$$

The resulting "Wavefront Compensation" control law is:

$$u_i = -G\hat{x}_i \tag{27}$$

Here the gain matrix G is:

$$G = \left[c_{wu} I + \left(\frac{\partial w}{\partial x_R} \frac{\partial x_R}{\partial u_R} \right)^T \frac{\partial w}{\partial x_R} \frac{\partial x_R}{\partial u_R} \right]^{-1} \left(\frac{\partial w}{\partial x_R} \frac{\partial x_R}{\partial u_R} \right)^T \frac{\partial w}{\partial x_R} \tag{28}$$

Using the OSE as part of the CCAT control has a great advantage – control decisions can be made based not just on the DOFs that are directly actuated, but in the context of all of the errors. This allows the controller to use actuation in the controlled DOFs to mitigate the optical effects of errors that are incurred in non-actuated DOFs. An example case is the lateral translation of a segment. Such a motion occurs when the base structure expands, and the consequence is a small but significant WFE, as the segment moves off of the ideal surface. This error occurs in a direction orthogonal to the 3DOFs along which the actuators act – yet by moving the segment in piston and tilt, the optical effects of this displacement can be partly corrected.

7. EXAMPLE

A simulation example is illustrated in Figures 4-6. This simulation run began with an initial segment state error randomly generated, with 50 um/50 urad standard deviation per axis, including the uncontrolled axes such as segment lateral translation, as shown in Figure 4. In the first cycle of the simulation the initial WFE was 67 nm. Using simulated LADD sensor measurements, the initial WFE was estimated by the OSE, with an estimation error of 5.6 um. The initial control was effective, dropping the WFE to 9 um; with addition of pointing control, WFE dropped to 2 um.

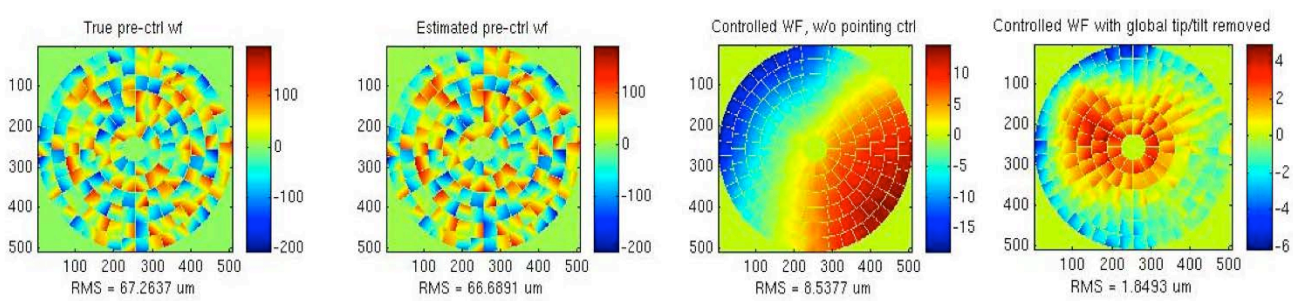

Figure 4. First time step, showing WFE before and after control, both without and with pointing control.

The performance over a series of 200 steps is summarized in Figure 5, which shows the WFE immediately before and after each control. The LADD sensors are utilized at each step; they are augmented by pointing measurements at every 10th time step as well. As shown, the pointing control is effective in limiting total WFE, as the LADD sensors alone are completely insensitive to global pointing modes. LADD sensor errors were 1 um 1 sigma per measurement axis; the 1 sigma process noise was 10 um and 10 urad.

The WFE for the 200th time step is shown in Figure 6: the starting WFE; the estimated starting WFE; and the WFE following LADD control and LADD plus pointing control.

The LADD control process is limited by several factors, including the geometry of the segments, the placement of the sensors, the sensor noise, and the various telescope disturbances. The work underway at Caltech and JPL will continue to explore performance of this sensor design and configuration.

This research was carried out at the Jet Propulsion Laboratory, California Institute of Technology, under a contract with the National Aeronautics and Space Administration.

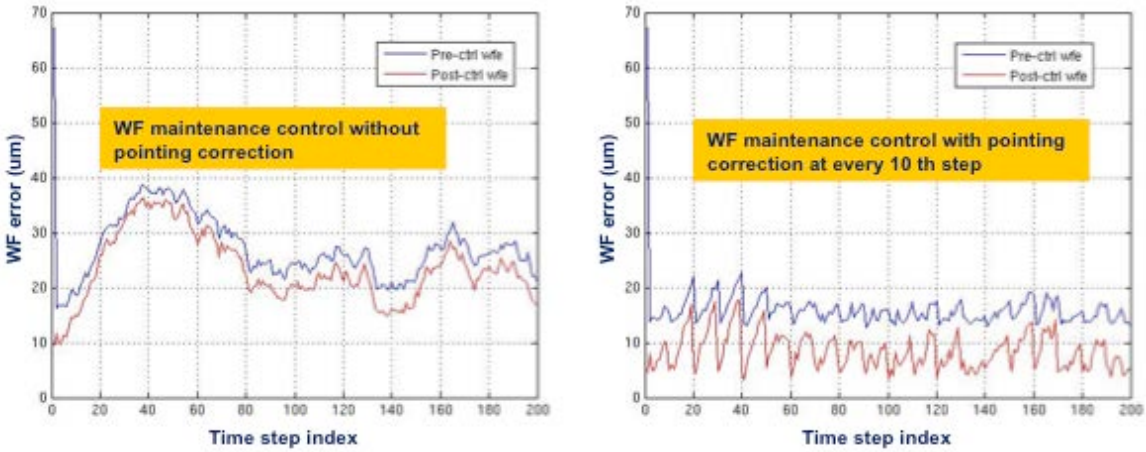

Figure 5. WF maintenance control example, using Wavefront Compensation controller. Plot on the left shows WF history without pointing correction; plot on the right includes pointing updates every 10th time step.

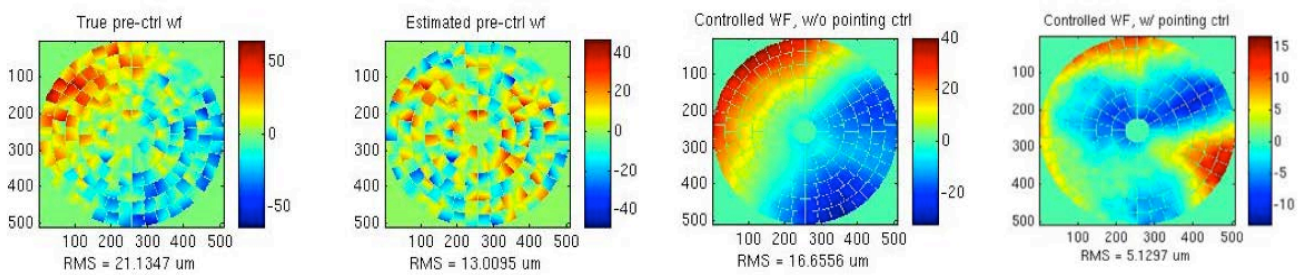

Figure 6. 200th time step, showing WFE before and after control, both without and with pointing control..

REFERENCES

[1] *Cornell Caltech Atacama Telescope (CCAT) Feasibility and Concept Design Study, Final Report* (2006).

[2] D. Redding, B. Breckenridge, Ken Lau, G. Sevaston, M. Levine and S. Shaklan, "Segmented Mirror Figure Control for a Space-Based Far-IR Astronomical Telescope," SPIE Vol. 1489, Structures Sensing and Control (1991).

[3] J.Z. Lou, A. Kissil, D. Redding, C.M. Bradford, S.Padin and D. Woody, "Modeling a Large Submillimeter-Wave Observatory," SPIE (2010).

[4] MACOS.

[5] D. Redding and W. Breckenridge, "Linearized Ray-Trace Analysis," Selected SPIE Papers on CD ROM, Volume 2, Lens Design, D. O'Shea, ed. (1998).

[6] A. Abramovici, "Electro-Optic Measurement of CCAT Segment-Segment and Primary-Secondary Relative Motions," JPL Internal Document (2009).

[7] E. Serabyn, T. Phillips and C. Masson, "Surface Figure Measurements of Radio Telescopes with a Shearing Interferometer," Applied Physics, Vol. 30, No. 10 (1991).

[8] A. Bryson and Y. Ho, *Applied Optimal Control*, Hemisphere Publishing (1975).